SCALING THE SECTIONAL DRAG PROFILE OF URBAN-CANOPY LAYERS

M Aguiar Ferreira
Department of Process & Energy
Delft University of Technology
Delft, the Netherlands
M.Ferreira@tudelft.nl

B Ganapathisubramani
Department of Aeronautics & Astronautics
University of Southampton
Southampton, UK
G.Bharath@soton.ac.uk

Introduction

There have been significant efforts towards improving predictions of the canopy drag of urban environments based on the surface geometry. Some of the most successful approaches are quasi-empirical formulations which treat urban agglomerates as a porous medium. Crucially, they make assumptions about the turbulence structure of the flow above and within the canopy which are still a target of intense scrutiny, partly because quality field and wind tunnel measurements are challenging to obtain, and few numerical simulations of large cube roughness proved to be sufficiently accurate. In this work, we investigate the mean flow characteristics of boundary layers developing over two staggered arrays of cuboids, with a uniform and a variable height distribution, in terms of velocity and pressure and assess the adequacy of these assumptions.

Profiles of the normalised velocity deficit and the streamwise turbulence intensity show a remarkable collapse with smooth-wall data at matching Re_τ, evidencing the presence of outer-layer similarity. The logarithmic regions are found to be fully immersed in the roughness sublayer, extending down to the height of the tallest obstacle. Although data in the canopy layer were partially missing, horizontally averaged statistics could still be obtained. Contrary to most formulations, the mean velocity profile within the canopy is not exponential, and the sectional drag coefficient and mixing length distributions cannot be considered constant. In light of these results and recent developments in urban canopy modelling, we propose a formulation for the sectional drag coefficient, taking advantage of the apparent self-similar behaviour of the axial-pressure difference across roughness elements.

Experimental methods

Experiments were conducted in the open-return, suction wind tunnel at the University of Southampton. This facility features a 7:1 contraction followed by a 4-m-long test section, 0.9 m wide and 0.6 m high. Boundary layers are established directly on the wind tunnel floor and develop under a nominally zero-pressure gradient. Hot-wire velocity measurements in the freestream show that the turbulence intensity remains lower than 0.2 % at 10 m/s. This work follows the convention that x, y, and z are the streamwise, wall-normal, and spanwise directions, respectively.

We investigate the boundary-layer flow developing over a staggered cube array with plan solidity $\lambda_P = 0.25$ (C10U) and an array of cuboids with the same plan arrangement but variable height distribution (C10R), illustrated in figure
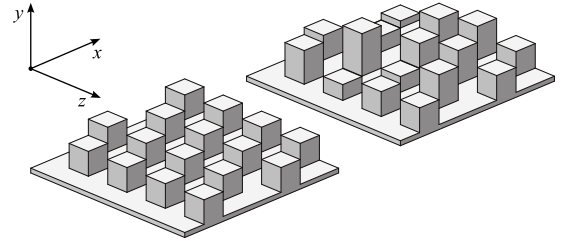

Figure 1: Perspective view of the staggered cube array with plan solidity $\lambda = 0.25$ (C10U), on the left, and the array of cuboids with the same plan arrangement but variable height distribution (C10R), on the right.

Table 1: Relevant parameters of the boundary-layer flow. The friction velocity U_τ was directly measured using a FE balance and the zero-plane displacement d^p was estimated from pressure data following Jackson's (1981) hypothesis.

Surface	C10U Exp.	C10U LC	C10R Exp.	C10R XCC
U_τ/U_0	0.0651	0.110	0.0689	0.0816
U_τ^p/U_0	0.0627	–	0.0678	–
d^p/H	0.619	0.617	0.735	0.710
H^+	440	600	465	391
Re_τ	5,288	4,800	6,091	3,910
y_0^+	39.9	60	53.7	37.1

1. At the measurement location, 3.3 m downstream of the contraction, the mean roughness height $H \approx 0.1\delta$, where δ is the boundary layer thickness. The wall shear stress was directly measured using a floating element balance, as detailed in Ferreira *et al.* (2018). Snapshots of planar particle image velocimetry (PIV) were acquired at different spanwise locations to obtain an accurate spatial representation of the flow field within the canopy. In contrast to previous studies (Cheng & Castro, 2002; Cheng *et al.*, 2007; Claus *et al.*, 2012), where the surface pressure was measured by pressure tapping opposite faces of individual roughness elements, the mean pressure field was estimated from in-plane velocity data and the surface value extrapolated from the nearest data point. As

discussed in Ferreira & Ganapathisubramani (2020), while this approach suffers from the missing out-of-plane components of velocity and acceleration, it still produces sensible estimates of surface pressure at a higher spatial resolution. Values of the frictional velocity U_τ and the zero-plane displacement height d (Jackson, 1981) for $C10U$, inferred assuming a constant spanwise distribution of the surface pressure, closely match direct measurements using the FE balance and a pressure-tapped roughness obstacle. Discrepancies are at worst 7% and 3.5%, respectively.

Additionally to experimental data, the present study also considers direct numerical simulations of channel flows over a series of cube arrays with varying λ_P by Leonardi & Castro (2010) and the large-eddy simulation of a channel flow over a geometrically similar array of cuboids to C10R by Xie *et al.* (2008). The relevant boundary-layer parameters are summarised in table 1.

Mean flow features

In this section, the basic properties of the boundary layer developing over each obstacle array are examined. Following the assessment of outer-layer similarity, the flow is considered in terms of inner scaling, whereby dynamically relevant roughness length scales and the zero-plane displacement height are estimated. Horizontal-averaged quantities over the canopy region and the mean pressure fields, at selected spanwise locations, are also presented here. These are compared against reported measurements and numerical solutions.

Outer-layer similarity

Canopy models rest on the principle of outer layer similarity of Townsend (1976), whereby turbulent motions outside the roughness sublayer (RS) become independent of viscosity and the surface condition. The velocity profile above the canopy may then be expressed by a standard log-wake function that scales appropriately. Not included for brevity, the scaled profiles of the horizontal-averaged velocity defect and turbulence intensity collapse for $y/\delta > 0.2$, evidencing the presence of outer layer similarity despite the large relative roughness height.

The extent of the RS has been regarded as an indicator of outer layer similarity (Ligrani & Moffat, 1986), yet it is unclear what relevant length scales determine its extent and there is no consensus on how to quantify it. The usual approach consists of identifying the blending height above which the flow is horizontally homogeneous. Following this definition, the depth of the RS is approximately $1.85H$ (0.15δ) for C10U and $2.5H$ (0.18δ) for C10R at the measurement location. While a larger penetration would inevitably introduce inhomogeneities farther away from the wall, even in extreme cases where $\delta/H = 5$ (Amir & Castro, 2011), the outer region may still conform to the usual universal profile. At the same time, studies have found roughness with much smaller heights that appeared to violate this hypothesis (Krogstad *et al.*, 1992; Bhaganagar *et al.*, 2004; Placidi & Ganapathisubramani, 2018), so it would be misleading to expect it to hold solely based on this criterion.

Several authors have attempted to find alternative, 'meaningful' indicators that embody the roughness effect on the mean flow. They are typically based on a ratio between the characteristic turbulent length scale in the outer region and that of the surface roughness, such as δ/H, δ/H_S or δ/y_0 (Jiménez, 2004; Flack *et al.*, 2005; Castro *et al.*, 2013), where H_S is the sand-grain roughness of Nikuradse (1950). Some of
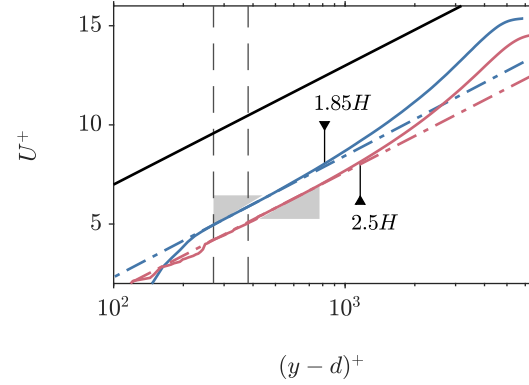

Figure 2: Horizontal-averaged, inner-scaled velocity profile over C10U (blue) and C10R (red). Dotted-dashed lines are the log-law fit through the data points in the inertial sublayer (highlighted grey) with a von Kármán constant $\kappa = 0.384$. The vertical dash lines indicate the maximum canopy height and the arrows the edge of RS. The solid-back line represents the smooth-wall log-law profile with negative wall intercept $A = -5$.

these criteria reliably predict outer layer similarity for different surfaces, but consistently fail for large obstacle arrays. Placidi & Ganapathisubramani (2018) recently argued that a suitable parameterisation must account, in addition to a relative measure of the roughness strength, for the nature of the canopy drag associated with the local surface topology, in which case it should consist of a combination of multiple parameters, rather than a single one. Their results suggest that, for large obstacle arrays, if the plan area of the sheltered region exceeds $\sim 20\%$ of the floor area of a repeating unit, then wall similarity is likely to hold provided that $\delta/H > 7$ and $\delta/H_S > 10$. This effect is quantified in Placidi & Ganapathisubramani (2018) by the sheltered solidity fraction $\lambda_S = (A_T - A_S)/A_T$, where A_T is the total plan area and A_S is the sheltered plan area. Particularly, $\lambda_S|_{C10U} = 0.5$ and $\lambda_S|_{C10R} = 0.62$ satisfy the condition $\lambda_S < 0.8$, and, since $\delta/H > 7$ and $\delta/H_S > 10$ are also verified, both cases meet the proposed requirements for wall similarity.

Boundary-layer parameters

The extent of the inertial sublayer (IS) and the height of the zero-plane displacement d were estimated by fitting the indicator function Ξ, using the von Kármán constant $\kappa = 0.384$ and U_τ from floating element measurements. Estimates of d as the log-law intercept compare well with those determined as the centroid of the surface drag, following Jackson's (1981) hypothesis. Both methods predict an increase due to height variability, and the discrepancy between them is at worse 8.5%.

The horizontal-averaged, viscous-scaled velocity profiles are shown in figure 2. Contrary to the traditional well-defined layer arrangement above the canopy, wherein the RS is followed by the IS, in turn preceding the outer region, the current analysis (based on the indicator function) suggests that the IS extends down to the top of the canopy and is fully immersed within the RS. This observation supports the hypothesis of Cheng & Castro (2002) that the horizontal-averaged velocity profile may assume a logarithmic behaviour where turbulence is predominantly influenced by the surface geometry. Furthermore, it suggests that using a logarithmic profile to set the velocity-continuity condition at the edge of

urban canopies, as in the models developed by Macdonald (2000), Coceal & Belcher (2004), Millward-Hopkins *et al.* (2011) and Yang *et al.* (2016), is a sensible approximation, especially for uniform arrays.

Within the canopy layer

Given the three-dimensional nature of the flow within the canopy layer, snapshots of the flow field were taken at different spanwise locations, and the flow statistics in the region with no optical access (behind out-of-plane obstacles) were linearly interpolated along the streamwise direction for C10U. A similar treatment could not be carried out for C10R owing to a substantial lack of data. All field variables within the canopy were extrinsically averaged over the total volume, as outlined in Böhm *et al.* (2013).

The horizontal-averaged velocity profile normalised by U_H is given in figure 3a. The data show a remarkable collapse with the direct numerical simulation (DNS) from Leonardi & Castro (2010), revealing a strong shear layer around the canopy top where the vertical velocity gradient is most intense. Incidentally, the velocity scaling U_H is inferred at this location, so its uncertainty is intrinsically high whether field or point measurement techniques are considered. In agreement with observations by Coceal & Belcher (2004) and Castro (2007), the velocity profile within the canopy does not exhibit exponential growth. This appears to be the case for all urban-like roughness, even those with a variable height distribution that are characterised by much lower velocity gradients. Equivalent measurements had previously been reported by Macdonald (2000) and Cheng & Castro (2002). They were either vertically unresolved or incomplete in the lower half of the canopy, and the velocity profile would appear to follow an exponential curve. Similarly, Castro (2017) showed that exponential velocity profiles may arise if a sufficiently coarse grid is used in numerical simulations.

The variation of the sectional drag coefficient C_D and the mixing length l_m within the canopy are shown in figures 3b and 3c, respectively. C_D is defined as

$$C_D(y) = \frac{2D(y)}{\rho |U(y)| U(y)}, \tag{1}$$

where $D(y) = \lambda_P \Delta p(y)$ is the canopy drag force per unit volume of air and Δp is the sectional drag profile (discussed in detail in the following section). l_m is given by

$$l_m = \frac{\sqrt{-\overline{uv}}}{\partial U/\partial y}. \tag{2}$$

In-plane and horizontal-averaged quantities still show similar trends, albeit to a lesser extent. There is a fairly good agreement between estimates of C_D. Specifically, the present measurements and DNS data collapse in the upper half of the canopy for $y/h > 0.7$. The values inferred from velocity data and surface pressure by Cheng & Castro (2002) are relatively higher, yet they still capture the general behaviour of the sectional drag coefficient, contrary to suggestions that the lowest data point could be an outlier (Coceal & Belcher, 2004), in which case it would appear to plateau. Constant C_D is a crucial assumption of urban-canopy models. However, by definition, it is likely to grow exponentially approaching the wall (refer to equation 1). The viability of this approximation has been rigorously examined by Castro (2017) for a range of packing densities and different plan arrangements, staggered and aligned. He stresses that unless $\lambda_P \leq 0.15$, assuming uniform distributions of C_D across the canopy is a clear
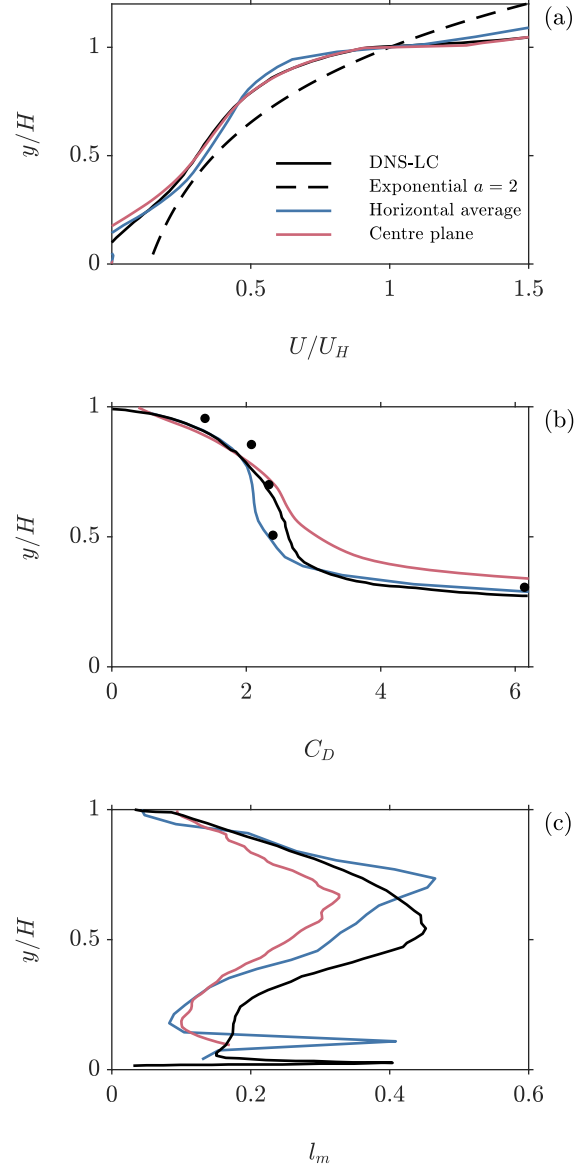

Figure 3: Flow statistics within the canopy of C10U, obtained by taking the streamwise average along the centre plane of the roughness obstacles (red) or taking the horizontal average over a repeating unit (blue). **(a)** Mean velocity profile normalised by the velocity at the top of the canopy layer $U_H = U(y/H = 1)$. **(b)** Sectional drag coefficient, as defined by equation 4.4. The canopy drag force was estimated from pressure data and normalised by the horizontal-averaged velocity field. Values inferred from velocity data and surface pressure from Cheng & Castro (2002) are included for reference. **(c)** mixing length scale given as the ratio $(-u'v')/(\partial U/\partial y)$.

oversimplification. Such is also the case of the mixing length scale, which peaks at around the mid-canopy height.

Scaling the sectional drag profile

Addressing the need to improve the current assumptions of canopy models, we examine whether the sectional drag profile Δp can be described by a functional relationship, governed by a combination of scaling laws. Yang *et al.* (2016) parameterise the wake geometry of individual roughness elements

based on the ratio of the horizontal convective velocity scale (U_h) to the turbulent transport velocity scale in the vertical direction (U_τ). They argue that the wake expansion rate behind solid objects, whose aspect ratio is on the order $\mathscr{O}(1)$ or lower, is primarily driven by $U_h^+ = U_h/U_\tau$ since the contribution to entrainment by the lateral shear layers is relatively small. Specifically, for a given obstacle array, the sheltered volume fraction within the canopy is proportional to U_h^+ and, consequently, so is the horizontal-averaged vertical velocity gradient. We may then interpret this quantity as a measure of the strength of the shear layer that is not explicitly dependent on τ_h. This is valid provided the plan solidity λ_P remains constant (i.e. varying the Reynolds number alone), or otherwise it must also be taken into account. For example, surfaces with different plan densities may have similar U_h^+, but the sparser would naturally have a less prominent shear layer over a repeating unit. Following this argument, the non-dimensional shear expressed by $G(\lambda_P, U_h^+)$, which contains information about the local Reynolds number and the mean velocity shear at the height of the obstacles, is investigated as an appropriate, useful scaling parameter for the sectional drag profile of urban canopies.

Figure 4 shows the sectional drag profile $\Delta p(y)$ of individual roughness elements within staggered-cube arrays of varying plan solidity and the array of cuboids C10R. Values are normalised by $\rho U_\tau^2/\lambda_P$, corresponding to the average contribution to surface drag across roughness elements. The pressure distribution over the windward side dominates the sectional drag profile. High-pressure regions typically develop near the top, where the velocity is higher, giving rise to a local maxima $(\hat{p}_u, \hat{y}_u)$ that falls in the range $0.8 - 0.9h$, where h is the local roughness height, as indicated in figure 5. The sectional drag becomes less significant towards the wall, reaching a local minimum $(\hat{p}_l, \hat{y}_l)$ before recovering to mean values. Although profiles can be markedly different, they show similar features, suggesting they could be described by a suitable functional expression using appropriately scaled parameters, namely the location and magnitude of the local extrema, $(\hat{p}_u, \hat{y}_u)$ and $(\hat{p}_l, \hat{y}_l)$, which effectively capture their general behaviour.

Shown in figure 5, the location and magnitude of the local extrema appear to scale well with $\lambda_P U_h^+$, which can interpreted as a measure of the intensity of the shear layer, showing a positive linear relationship. Notably, the slope of the linear regression of $\hat{p}_u$ is steeper than that of $(\hat{p}_u - \hat{p}_l)$, which implies that for a given fetch δ/H and fixed Re_τ, increasing U_h (e.g. by increasing the local roughness height) mostly comes with an increase in $\hat{p}_u$. Another interpretation could be that the sectional drag profile gradually becomes more uniform across the canopy the less prominent the shear layer is. This is the case of the shorter roughness elements within C10R. The relationship between the height of the local extrema and the significance of the shear layer is comparably weaker. As shown in figures 5c and 5d, the data does not follow a clear trend. Other factors besides the strength of the shear layer may also be important yet cannot be readily identified. Note that $\hat{y}_u$ is expected to plateau near the top of the roughness element since the pressure field above the canopy takes on the value of the freestream static pressure (i.e. $\Delta p = 0$ at $y/h = 1$). This boundary condition sets the upper limit for $\hat{y}_u$, necessarily lower than 1. Given the small dispersion of the data around the mean value, we assume, for modelling purposes, $\hat{y}_u = 0.85 \pm 0.05$. The position of the local minima $\hat{y}_l$ appears to be driven by the size of the frontal recirculating region, which develops upstream of the roughness obstacles and imposes a low-pressure value on the windward face.
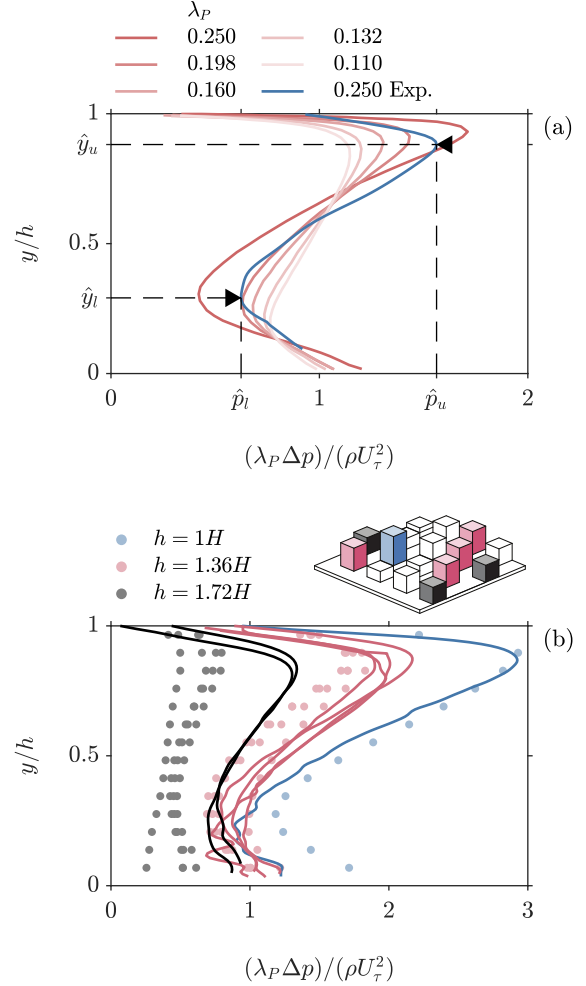

Figure 4: Sectional drag profile relative to the average drag produced by an individual roughness element $\rho U_\tau^2/\lambda_P$. **(a)** Uniform cube array with varying solidity fraction. Blue-coloured line represents the sectional drag derived from field pressure data normalised by U_τ as measured using the FE balance. Red-shaded lines correspond to DNS data from (Leonardi & Castro, 2010). The arrows indicate the local extrema $(\hat{p}_u, \hat{y}_u)$ and $(\hat{p}_l, \hat{y}_l)$. **(b)** Array of cuboids of variable height. Solid lines represent the sectional drag derived from pressure field data, colour-coded based on local height as shown in the top-right corner. Circles correspond to LES data from Xie *et al.* (2008).

Modelling aspects

The scaling arguments outlined above offer a pathway to derive a functional expression for the sectional drag profile of individual roughness elements. However, a meaningful scaling factor for the height of the local minima $\hat{y}_l$ is still missing. Assuming the size of the recirculating region is governed by mutual sheltering effects, $\hat{y}_l$ may be estimated by a geometric wake-sheltering model, such as that of Millward-Hopkins *et al.* (2013) and Yang *et al.* (2016). These simplified models establish a sheltered region of low momentum and an unsheltered region characterised by the horizontal convective velocity scale U_h. The degree of wake sheltering is quantified by the equivalent sheltered-layer height for arbitrary arrays, h_s, ranging form unsheltered to fully sheltered $0 < h_s < 1$. This length scale is determined by the wake geometry of the roughness element, which is a function of the width,
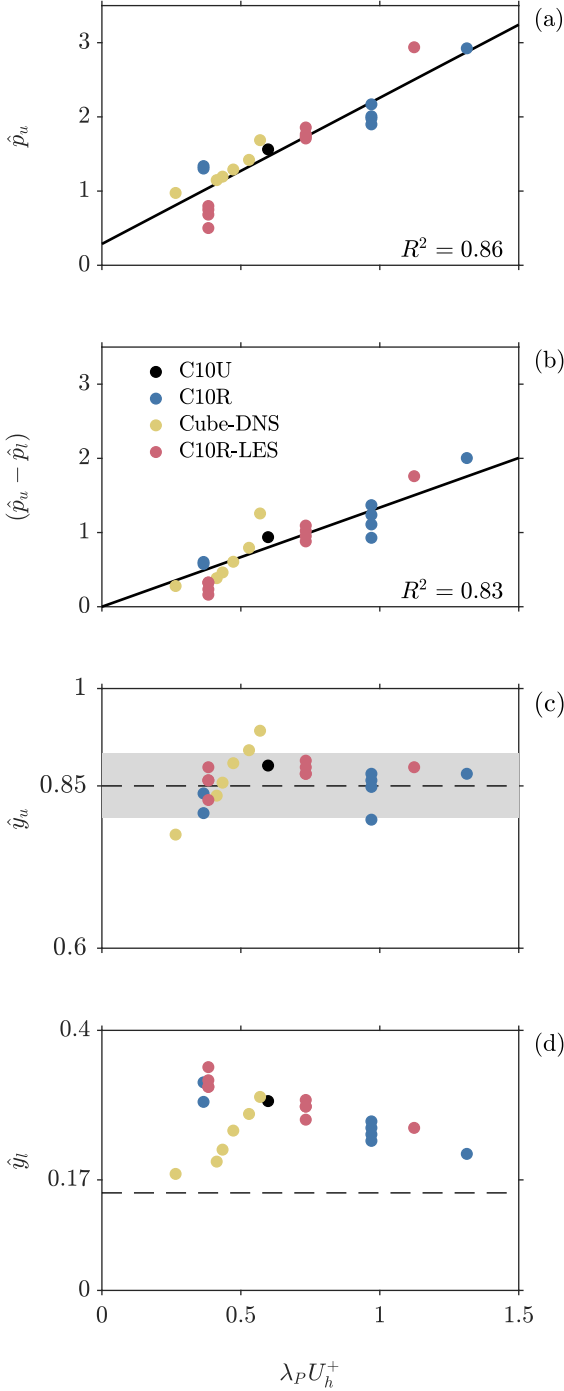
Figure 5: Empirical correlations for the sectional drag parameters. **(a)** Magnitude of the local maxima $\hat{p}_u$, **(b)** the peak-to-peak amplitude $(\hat{p}_u - \hat{p}_l)$, **(c)** position of the local maxima, and **(d)** position of the local minima normalised by the local roughness height h, upon $\lambda_P U_h^+$, interpreted here as a measure of the significance of the shear layer.
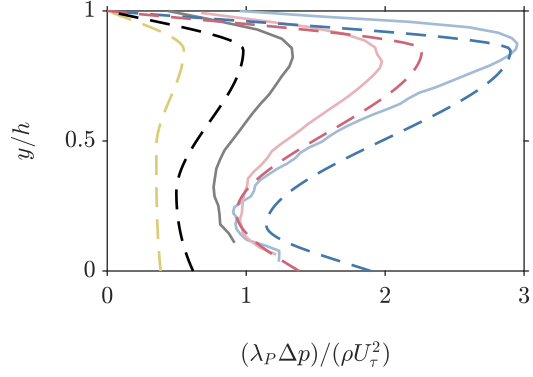

Figure 6: Estimated drag profiles of selected obstacles in C10R. Dashed lines are cubic splines in three pieces with zero-derivatives at the local extrema (equation 3), specified via empirical correlations depicted in figure 5. $\hat{y}_l$ was set to $0.25H$. Solid lines are the corresponding profiles obtained from pressure data.

Considering a piecewise third-order polynomial function (i.e. cubic spline) with zero derivatives at the local extrema for F, The ith piece of the 1-dimensional spline through points $[0, \hat{y}_l, \hat{y}_u, 1]$ is represented by

$$\hat{p}_i = \lambda \Delta p_i^+ = a_i + b_i \hat{y} + c_i \hat{y}^2 + d_i \hat{y}^3,$$

with

$$\frac{d\hat{p}}{d\hat{y}}(\hat{y}_u) = \frac{d\hat{p}}{d\hat{y}}(\hat{y}_l) = 0. \quad (3)$$

$\hat{p}_u$, $\hat{p}_l$, and y_u are given by the empirical correlations defined in figure 5, while y_l would be governed by h_s from the wake sheltering model. The boundary condition at the wall $\hat{p}_i(0) = \hat{p}_l + C_w(h/H)(\hat{p}_u - \hat{p}_l)$. This linear model is a function of the relative height distribution h/H, ensuring that $\hat{p}_i(0)$ is always greater than $\hat{p}_l$. The coefficient $C_w = 1/4$ was adjusted to yield the best fit of the shape function to the sectional drag profile of a roughness element of average height ($1H$). The estimates depicted in figure 6 were obtained by taking into account the spatially-averaged velocity distribution over C10R and the value of friction velocity. Using the correlations derived above, these quantities allow to determine the local extrema for each roughness element, except for $\hat{y}_l$ that we set to $0.25H$ for illustration purposes — if $\hat{y}_u < \hat{y}_l$, then $\hat{y}_l = \hat{y}_u$ and $\lambda \Delta p_l^+ = \lambda \Delta p_u^+$. Otherwise, $\hat{y}_l$ would have been estimated from a wake-sheltering model.

The functional relationship outlined above adequately reproduces the profiles of sectional drag across the entire canopy height. Discrepancies with results from pressure reconstruction arise from the spread of the data around the regression lines in figure 5. Setting $\hat{y}_l$ to $0.25H$ does not seem to have a significant impact on the quality of the reconstructed profiles. Based on the contribution of the largest roughness elements, partially sheltered and unsheltered, which contribute to nearly 90% of the total pressure drag, the zero-plane displacement $d/H = 0.75$. This value is only marginally higher than that obtained directly from pressure data (refer to table 1) and lower values would have been expected had the shortest obstacles been accounted for. Besides U_h^+, the distribution of surface drag could also be determined by specifying the value of the friction velocity U_τ, yielding an average relative error of approximately 20%.

height, and the wake-expansion rate), as well as the planar arrangement and height distribution of the surface roughness. The sheltered-layer height h_s effectively captures the impact of surface geometry on the canopy-flow topology and could potentially be used to estimate the location of the local minima $\hat{y}_l$. It then follows that $\Delta p^+ = F(\lambda U_\tau^+, h_s)$ can be used as a shape function for the axial pressure difference across individual roughness elements.

1 Summary

Scaled profiles of the horizontally-averaged axial velocity and turbulent intensity revealed the existence of outer-layer similarity for $y/H > 0.2$, despite the large relative roughness height. The IS is fully immersed within the RS and persists down to the edge of the canopy for both surfaces. Estimates of the displacement height defined as the origin of the log-law compare well with those determined as the centroid of the surface drag. Both methods predict an increase due to height variability and the discrepancy between them is at worse 8.5%. The horizontal-average velocity profile within the canopy layer does not exhibit an exponential behaviour, and both the sectional-drag coefficient and the mixing length vary significantly.

The normalised axial-pressure difference across individual roughness obstacles exhibits a self-similar behaviour that can be described by a functional expression parameterised by the local extrema $(\hat{p}_l, \hat{y}_l)$ and $(\hat{p}_u, \hat{y}_u)$. Based on scaling arguments, we established correlations for the location and intensity of these peaks. The non-dimensional shear factor (at the obstacle height) $\lambda_P U_h^+$ was shown to be a relevant parameter that linearly scales the intensity of the local extrema $\hat{p}_l$ and $\hat{p}_u$. The height of the local maxima $\hat{y}_u$, in turn, varies marginally with $\lambda_P U_h^+$, and the experimental and DNS datasets exhibit distinct trends, indicating that other factors might also play a role. Results further suggest that the size of the recirculating region on the windward face of the cuboids is the driving parameter for the height of the local minima $\hat{y}_l$. It is thus highly dependent on the surface geometry, including the shape of the obstacles, the plan arrangement and the relative height distribution. It is argued that $\hat{y}_l$ is associated with mutual sheltering effects and could possibly be parameterised by a geometric wake-sheltering model, such as that of Yang *et al.* (2016). Using a three-piece cubic spline and assuming a fixed $\hat{y}_l$, the normalised sectional-drag profile of individual roughness obstacles and surface drag distribution over C10R could be reproduced, and showed a good qualitative agreement with pressure data.

REFERENCES

Amir, Mohammad & Castro, Ian P 2011 Turbulence in rough-wall boundary layers: universality issues. *Experiments in fluids* **51** (2), 313–326.

Bhaganagar, Kiran, Kim, John & Coleman, Gary 2004 Effect of roughness on wall-bounded turbulence. *Flow, turbulence and combustion* **72** (2-4), 463–492.

Böhm, Margi, Finnigan, John J, Raupach, Michael R & Hughes, Dale 2013 Turbulence structure within and above a canopy of bluff elements. *Boundary-layer meteorology* **146** (3), 393–419.

Castro, Ian P 2007 Rough-wall boundary layers: mean flow universality. *Journal of Fluid Mechanics* **585**, 469–485.

Castro, Ian P 2017 Are urban-canopy velocity profiles exponential? *Boundary-Layer Meteorology* **164** (3), 337–351.

Castro, Ian P, Segalini, Antonio & Alfredsson, P Henrik 2013 Outer-layer turbulence intensities in smooth-and rough-wall boundary layers. *Journal of Fluid Mechanics* **727**, 119–131.

Cheng, H & Castro, Ian P 2002 Near wall flow over urban-like roughness. *Boundary-Layer Meteorology* **104**, 229–259.

Cheng, H., Hayden, P., Robins, A.G. & Castro, I.P. 2007 Flow over cube arrays of different packing densities. *Journal of Wind Engineering and Industrial Aerodynamics* **95** (8), 715–740.

Claus, Jean, Krogstad, P-Å & Castro, Ian P 2012 Some measurements of surface drag in urban-type boundary layers at various wind angles. *Boundary-Layer Meteorology* **145**, 407–422.

Coceal, O & Belcher, SE 2004 A canopy model of mean winds through urban areas. *Quarterly Journal of the Royal Meteorological Society* **130** (599), 1349–1372.

Ferreira, M Aguiar & Ganapathisubramani, Bharathram 2020 Piv-based pressure estimation in the canopy of urban-like roughness. *Experiments in Fluids* **61** (3), 70.

Ferreira, M A, Rodríguez-López, Eduardo & Ganapathisubramani, B 2018 An alternative floating element design for skin-friction measurement of turbulent wall flows. *Experiments in Fluids* **59**, 155.

Flack, Karen A, Schultz, Michael P & Shapiro, Thomas A 2005 Experimental support for townsend's reynolds number similarity hypothesis on rough walls. *Physics of Fluids* **17** (3), 035102.

Jackson, PS 1981 On the displacement height in the logarithmic velocity profile. *Journal of fluid mechanics* **111**, 15–25.

Jiménez, Javier 2004 Turbulent flows over rough walls. *Annu. Rev. Fluid Mech.* **36**, 173–196.

Krogstad, P-Å, Antonia, RA & Browne, LWB 1992 Comparison between rough-and smooth-wall turbulent boundary layers. *Journal of Fluid Mechanics* **245**, 599–617.

Leonardi, Stefano & Castro, Ian P 2010 Channel flow over large cube roughness: a direct numerical simulation study. *Journal of Fluid Mechanics* **651**, 519–539.

Ligrani, Phillip M & Moffat, Robert J 1986 Structure of transitionally rough and fully rough turbulent boundary layers. *Journal of Fluid Mechanics* **162**, 69–98.

Macdonald, RW 2000 Modelling the mean velocity profile in the urban canopy layer. *Boundary-Layer Meteorology* **97** (1), 25–45.

Millward-Hopkins, JT, Tomlin, AS, Ma, L, Ingham, D & Pourkashanian, M 2011 Estimating aerodynamic parameters of urban-like surfaces with heterogeneous building heights. *Boundary-Layer Meteorology* **141** (3), 443–465.

Millward-Hopkins, JT, Tomlin, AS, Ma, L, Ingham, DB & Pourkashanian, M 2013 Aerodynamic parameters of a uk city derived from morphological data. *Boundary-layer meteorology* **146** (3), 447–468.

Nikuradse, Johann 1950 *Laws of flow in rough pipes*. National Advisory Committee for Aeronautics Washington.

Placidi, M & Ganapathisubramani, B 2018 Turbulent flow over large roughness elements: Effect of frontal and plan solidity on turbulence statistics and structure. *Boundary-Layer Meteorology* **167**, 99–121.

Townsend, A A 1976 *Structure of Turbulent Shear Flow*, 2nd edn. Cambridge University Press.

Xie, Zheng-Tong, Coceal, Omduth & Castro, Ian P 2008 Large-eddy simulation of flows over random urban-like obstacles. *Boundary-layer meteorology* **129** (1), 1.

Yang, Xiang I. A., Sadique, Jasim, Mittal, Rajat & Meneveau, Charles 2016 Exponential roughness layer and analytical model for turbulent boundary layer flow over rectangular-prism roughness elements. *Journal of Fluid Mechanics* **789**, 127–165.